International Research Journal of Engineering and Technology (IRJET) e-ISSN: 2395 -0056
Volume: 02 Issue: 09 | Dec-2015 www.irjet.net p-ISSN: 2395-0072

Lateral shearing interferometer with Zernike mode for wavefront error analysis

M.Mohamed Ismail [1] M.Mohamed Sathik [2].

Research Scholar, Department of Computer Science, Sadakathullah Appa College, Tirunelveli, Tamilnadu, India [1]
Principal, Sadakathullah Appa College, Tirunelveli, Tamilnadu, India. [2]

Abstract - ***This paper presents a new Zernike base phase screen generation with known, realistic and repeatable characteristics. We proposed a new method for Zernike based phase screen for shearing interferometer. The interference fringe pattern distorted due to the Zernike based phase screen is demonstrated. This method of phase screen generation is validated through a simulated experiment which extracts the phase from the distorted wavefront using Window Fourier Transform method.***

Key Words: *Adaptive Optics, Shearing Interferometer, Zernike Polynomial, Phase Screen.*

I) INTRODUCTION

In recent years, astronomers have developed the technique of Adaptive Optics (AO) [1] to actively sense and correct wavefront distortions at the telescope during observations. A telescope with adaptive optics measures the wavefront distortions with a wavefront sensor and then applies phase corrections with a deformable mirror [2] on a time scale comparable to the temporal variations of the atmosphere's index of refraction. Adaptive Optics dramatically improves image resolution and increases the image coherence.

A wavefront sensor based on polarization shearing interferometry (PSI) [3] technique has been developed. Lateral shearing interferometry was employed as the wavefront sensor for real time atmospheric corrections [4, 5]. The PSI combines the wavefront with a shifted version of itself to form interference. A shearing device splits the incoming wavefront into two components and shifts one of them. The two wavefronts are mutually displaced by a distance s, called shear. They interfere in their overlap area. By their position, the interference fringes are a measure of the phase difference over the shear distance in the shear direction. A detailed theory on the use of this PSI device as a wavefront sensor for Adaptive Optics applications is provided [6, 7].

We simulated a shearing interferometer fringe pattern based on Zernike polynomials and later errors caused due to atmospheric turbulence were incorporated by Zernike base phase screen. Due to presence of noise in the interferogram, fringe pattern image is distorted and it is important to retrieve phase information from fringes for further process of wavefront error estimation.

II Interference Fringe Pattern Simulations using Zernike Polynomial

The basic interferometric equation is given in 2.1 and the gradient of the Zernike polynomial is represented by equation 2.2

$$I = K_0 + K_1 \cos\left(\frac{2\pi}{\lambda}\Delta W(x,y)\right) \qquad (2.1)$$

$$\Delta Z_j = \sum_{j'} \gamma_{jj'} Z_{j'} \qquad (2.2)$$

Where $\gamma_{jj'}$ are the coefficients of the Zernike expansion in the j^{th} derivative of the Zernike. The matrix γ is called Zernike derivative matrix and it is given in Noll[8]. And the wavefront slope is explicitly written as

$$\Delta W(x,y) = \sum_{j=1}^{n} a_j \left(s \sum_j \gamma_{x_{jj}} Z_j + t \sum_j \gamma_{y_{jj}} Z_j \right) \qquad (2.3)$$

The interferogram are simulated with Zernike coefficients, and for different values of the Zernike coefficients it represents different aberrations. The figure 1 shows the simulated interference fringe pattern using only defocus term while making all other coefficients zero. The low order Zernike polynomials is shown in the Table 1.

j	n	m	$Z_j(\rho, \theta)$	Meaning
1	0	0	1	Piston
2	1	1	$2\rho\cos\theta$	Tilt along X
3	1	1	$2\rho\sin\theta$	Tilt along Y
4	2	0	$\sqrt{3}\ 2\rho^2 - 1$	Defocus
5	2	2	$\sqrt{6}\rho^2 \sin 2\theta$	3rd Order Astigmatism - X ;
6	2	2	$\sqrt{6}\rho^2 \cos 2\theta$	3rd Order Astigmatism - Y ;
7	3	1	$\sqrt{8}\,3\rho^3 - 2\rho \sin 2\theta$	3rd Order Primary Coma - X
8	3	1	$\sqrt{8}\,3\rho^3 - 2\rho \cos 2\theta$	3rd Order Primary Coma - Y
9	3	3	$\sqrt{8}\rho^3 \sin 3\theta$	3rd Order Triangular Coma - X
10	3	3	$\sqrt{8}\rho^3 \cos 3\theta$	3rd Order Triangular Coma - Y
11	4	0	$\sqrt{5}(6\rho^4 - 6\rho^2 + 1)$	3rd Order Spherical

Table 1: Zernike polynomials

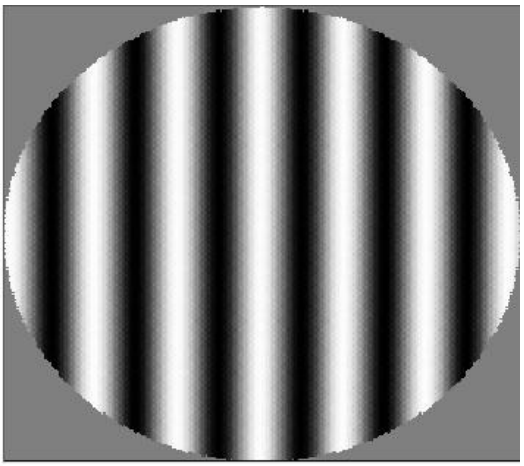

Figure 1: Simulated PSI interferogram using the Zernike coefficients

III) Zernike-based Phase Screen

Noll [8] has introduced a normalization for the Zernike polynomials that is perfectly suited for application of Kolmogorov turbulence. The use of Zernike polynomials for describing the aberrations introduced by the atmospheric turbulence is reviewed [9]. The derivatives of the Zernike Polynomials can be written as a linear combination of Zernike polynomial. Zernike polynomials are widely used for describing the classical aberrations of an optical system. They have the advantage that the low order polynomials are related to the classical aberrations like spherical aberration, coma and astigmatism. Fried [10] used these Zernike polynomials to describe the statistical strength of aberrations produced by the atmospheric turbulence. Zernike polynomials are a set of orthonormal polynomials, defined on a unit circle and hence are used to express the turbulent wavefront in the circular aperture telescope. Normalization for the Zernike polynomials that is perfectly suited for application of Kolmogorov turbulence is used. The Zernike polynomials are usually written in polar form ρ and θ. Zernike polynomial approach does not begin with a random phase array, instead the coefficients are combined into two-dimensional random functions. In [8] it is defined a new modified set of Zernike polynomials $Z_j(p, \theta)$ and these polynomials to be

$$Z_{even\ j} = \sqrt{n+1}R_n^m(r)\sqrt{2}\cos(m\theta), \qquad m \neq 0,$$

$$Z_{odd\ j} = \sqrt{n+1}R_n^m(r)\sqrt{2}\sin(m\theta), \qquad m \neq 0,$$

$$Z_j = \sqrt{n+1}R_n^0(r), \qquad m = 0, \tag{3.1}$$

The functions $R_n^m(r)$ are referred to as radial functions defined to be

$$R_n^m(r) = \sum_{s=0}^{(n-m)/2} \frac{(-1)^s (n-s)!}{s![n+m/2-s]![n-m/2-s]!} r^{n-2s} \tag{3.2}$$

Based on a polar coordinate system, R is the radius, ρ is the position along the radius, and θ is the angle with respect to the x-axis. Noll's numbering sequence of the index j corresponds to each polynomial Z_j and proceeds by row. The given value of radial degree n, increases with azimuthal frequency m. We generate random phase screens, θ_{atm} from the relationship: According to Noll's numbering system, j is used instead of n, the radial order and m, the azimuthal order. The two indices m and n are whole numbers satisfying m ≤ n and n − m is even. The total number of modes up to a given radial order is therefore *Jn = (n+1) (n+2) / 2* . The low order Zernike polynomials, where the columns and rows indicate azimuthal and radial order respectively is given. The polynomial expansion of an arbitrary wavefront over the unit circle is defined as

$$\Phi(R\rho,\theta) = \sum_j a_j Z_j(\rho,\theta), \tag{3.3}$$

with $\rho = r/R$ and the coefficients a_j being given by

$$a_j = \int d^2\rho\, W(\rho)\phi(R\rho,\theta) Z_j(\rho,\theta) \tag{3.4}$$

Since Zernike polynomials have the unique property of representing each mode individually, one can estimate the contributions by the atmosphere by estimating the individual Zernike terms. The propagation of a wave through the atmosphere and the structure function for the phase fluctuations is defined as

$$D_\phi(r) = 2[\langle\phi^2(r_1)\rangle - \langle\phi(r_1)\phi(r_1+r)\rangle] \tag{3.5}$$

For Kolmogorov turbulence D(r), can be written in terms of the correlation length as

$$D_\phi(r) = 6.88\left(\frac{r}{r_0}\right)^{5/3} \tag{3.6}$$

The structure function is related to the Weiner spectrum, $\phi(k)$ by

$$D_\phi(r) = 2\int dk\,\phi(k)[1-\cos(2\pi k.r)] \tag{3.7}$$

By using Eq. (2.28) and the integral

$$\int_0^\infty x^{-p}[1-J_0(bx)]dx = \frac{\pi b^{p-1}}{2^p[\Gamma(p+1)/2]^2\sin[\pi(p-1)/2]} \tag{3.8}$$

We find that,

$$\phi(k) = (0.023/r_0^{5/3})k^{-11/3} \tag{3.9}$$

This is the Wiener spectrum of the phase fluctuations due to Kolmogorov turbulence. A Zernike representation of this spectrum can be obtained by evaluating the covariance of the expansion coefficients in Eq. (3.3). The coefficients a_j can be considered to be Gaussian random variables with zero mean so that the covariance is, from Eq. (3.4),

$$\langle a_j^* a_{j'}\rangle = \int d\rho \int d\rho' W(\rho)W(\rho') Z_j(\rho,\theta) \times C(R\rho,R\rho')Z_{j'}(\rho',\theta') \tag{3.10}$$

Where $C(R\rho,R\rho')$ is the phase covariance function

$$C(R\rho,R\rho') = \langle\phi(R\rho)\phi(R\rho')\rangle \tag{3.11}$$

Equation (3.10) can also be written in Fourier space as

$$\langle a_j^* a_{j'}\rangle = \int\int dk dk' Q_j^*(k)\phi(k/R,k'/R)\,Q_{j'}(k') \tag{3.12}$$

Where,

$$\phi(k/R,k'/R) = 0.023(R/r_0)^{5/3}k^{-11/3}\delta(k-k')$$

Substituting Eq(3.11) into Eq.(3.12) yields

$$\langle a_j^* a_{j'} \rangle = (0.046/\pi)(R/r_0)^{5/3}[(n+1)(n'+1)]^{1/2}$$

0.00
0.00
0.00
5.00
-2.0031
-1.0025
1.0069
2.0011
-1.0043
-1.0056
1.0093

$$\times (-1)^{(n+n'-2n)/2}\delta mm' \times \int dk\, k^{-8/3}\frac{J_{n+1}(2\pi k)J_{n'+1}(2\pi k)}{k^2} \quad (3.13)$$

It is a Zernike matrix representation of the Kolmogorov phase spectrum. This representation has the advantage that the integrals that appear in Eq. (3.13) can be evaluated in closed form.

For our experiment we used Zernike based phase screen for a turbulence generator with known, realistic, and repeatable characteristics. It is used to characterize the phase estimation, data reduction methods and error finding by comparing the input values of Zernike coefficients (which we used for generating Zernike based phase screen) and output of Zernike values (which we get after phase estimation and data reduction). The comparison of input Zernike and output Zernike depends on the performance of the phase extraction algorithm and data reduction method. We have generated an interferogram with known 11 Zernike coefficients of Kolmogorov turbulence and Gaussian Noise. We generated an interferogram by keeping only spherical and defocus and it is shown in figure 3. We generated an interferogram with known 11 Zerrnike coefficients which is shown in figure 4.A with added Kolmogorov turbulence and Gaussian noise is shown in figure 4.B. In table 2 we have given the values of 11 Zernike coefficients and the Kolmogorov turbulence of D/r_0 =1 and Gaussian noise of 0.5 where D – Telescope Diameter and r_0- Fried Parameter.

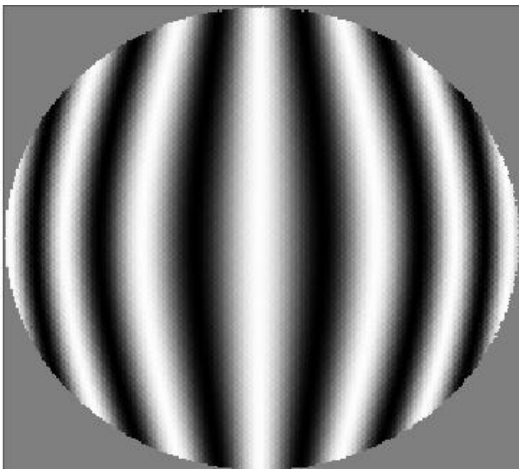

Figure 3: A Interferogram with Spherical Aberration & Defocus

Table 2. Input Zernike Coefficients

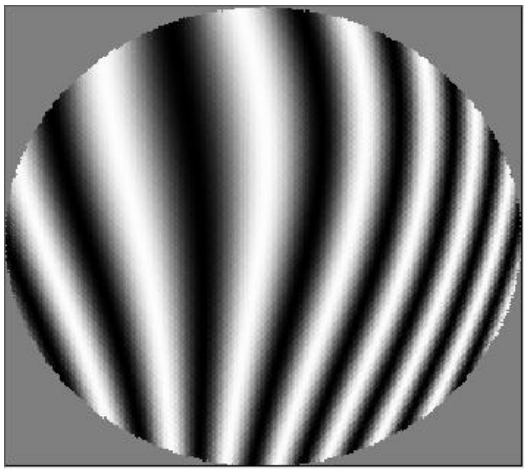

(A)

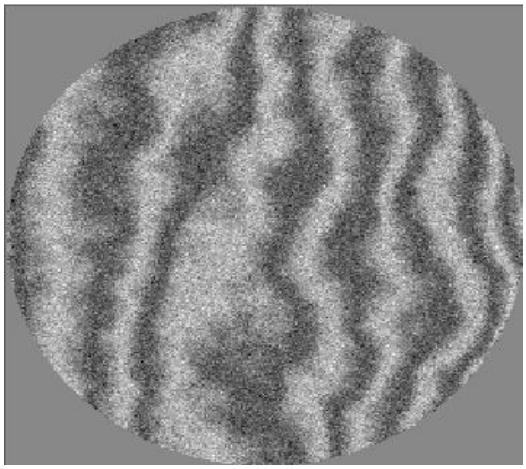

(B)

Figure 4: (A) All 11 Zernike Coefficients based Interferogram (B) including Kolmogorov turbulence and Gaussian noise

IV) Phase Extraction through Windowed Fourier Transform

Noise is an unwanted signal which is corrupting the original signal and to retrieve phase from the interferogram we need to denoise the fringe pattern. Noise degrades the quality of the information of original signal. The interferogram needs to be processed before it can be used for computing the phase aberration. Image denoising involves the manipulation of the image data to produce a visually high quality image. There are various methods of noise reduction in practice. There are many applications to the noise control based on signal types. In this report, we consider three de-noising methods, the traditional Filtering method, Fourier technique and the wavelet denoising method to perform their comparative study. Different noise models including additive and multiplicative types are used. They include Gaussian noise and Kolmogorov turbulence phase.

The procedure for computing Windowed Fourier Transform (WFT) is to divide a longer time signal into shorter segments of equal length and then compute the Fourier transform separately on each shorter segment. This reveals the Fourier spectrum on each shorter segment. The windowed Fourier transform also called the Short Time Fourier Transform (STFT), or the sliding Fourier transform which partitions the time-domain input signal into several disjointed or overlapped blocks by multiplying the signal with a window function and then applies the discrete Fourier transform to each block.

The magnitude square of the Fourier transform is the energy density spectrum at time *t*. By varying *t,* we obtain a two dimension density of time and frequency called the spectrogram. Window functions, also called sliding windows in which the amplitude tapers gradually and smoothly toward zero at the edges. Because each block occupies different time periods, the resulting WFT indicates the spectral content of the signal at each corresponding time period. By moving the sliding window one can obtain the spectral content of the signal over different time intervals. The WFT is a function of time and frequency that indicates the spectral content of a signal evolves over time. A complex-valued, 2-D array called the STFT coefficients stores the results of windowed Fourier transforms. The magnitudes of the STFT coefficients form a magnitude time-frequency spectrum, and the phases of the STFT coefficients form a phase time-frequency spectrum. The WFT is one of the most straightforward approaches for performing time-frequency analysis helps us to easily understand the concept of time-frequency analysis. The WFT is computationally efficient because it uses the Fast Fourier transform (FFT) [11, 12 and 13].

For phase estimation, we fitted a one dimensional noisy fringe pattern to the windowed Fourier transform which transformed into spectrum. The noise permeates the whole spectrum domain with very small coefficients due to its randomness and incoherence with the WFT basis. This is suppressed by discarding the spectrum coefficients if their amplitudes are smaller than a preset threshold. A smooth image is produced after an Inverse Windowed Fourier Transform (IWFT).

The WFT and IWFT can be written as [14, 15]

$$Sf(u,\xi) = \int_{-\infty}^{\infty} f(x)\, g(x-u)\, \exp(-j\xi x)\, dx, \tag{4.1}$$

$$f(x) = \frac{1}{2\pi} \int_{-\infty}^{\infty} \int_{-\infty}^{\infty} Sf(u,\xi)\, g(x-u)\, \mathrm{X} \exp(j\xi x)\, d\xi du \tag{4.2}$$

Where $Sf(u,\xi)$ denotes the WFT spectrum; $g(x)$ is a window, which can be chosen as a Gaussian function,

$$g(x) = \exp(-x^2/2\sigma^2) \tag{4.3}$$

In a Fourier transform, when $f(x)$ is transformed to Ff(ξ), the frequency information is maintained but time information is lost and can hardly be recognized i.e., Ff(ξ) it is possible to find frequencies that appear from the

spectrum, but not where they occur in the signal. But using WFT $Sf(u,\xi)$ it is possible to know not only the spectrum components but also component that appears in the time domain. The WFT has advantages over Fourier transform as it is performed over a local area. It is determined by the extension of *g(x)*, where a signal in one position will not affect the signal in another position. In spectral analysis also the spectrum of the signal in a local area is simpler than the spectrum of the whole field signal hence more effective operation of the spectrum is possible.

4.1 Steps employed for phase Extraction using Windowed Fourier Transforms

1. A code for a straight fringe in the interferometer is developed using LabVIEW.

2. Due to inclusion of turbulence (Zernike based phase screen) the fringe pattern gets distorted. On the application of different types of error, the fringes get distorted in a different way.

3. The one-dimensional plot of the distorted fringe pattern is taken into account for easy analysis.

4. The Windowed Fourier Transform Technique is applied to the one-dimensional plot which transforms into spectrum.

5. In spectrum domain, the noises are eliminated by discarding the spectrum coefficients of their amplitudes which are smaller than a preset threshold.

6. A smooth image is produced after an IWFT.

The figure 5.A shows that the noisy interferogram with Gaussian noise of 0.5 and its filtered image is shown in figure 5.B using windowed Fourier transform The figure 5.C shows that the noisy interferogram affected by zernike based turbulent phase screen of D/r_0 ratio =0.5 with Gaussian noise of 0.5 and its filtered image is shown in figure 5.D using windowed fourier transform by above developed algorithm.

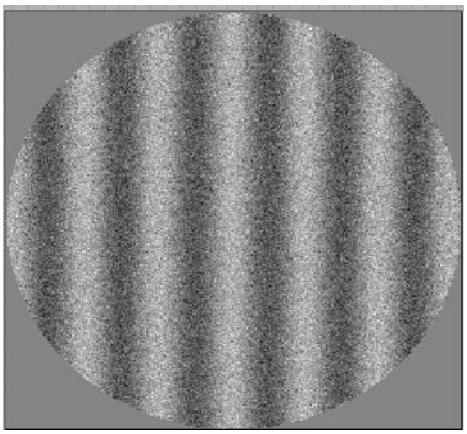

(A)

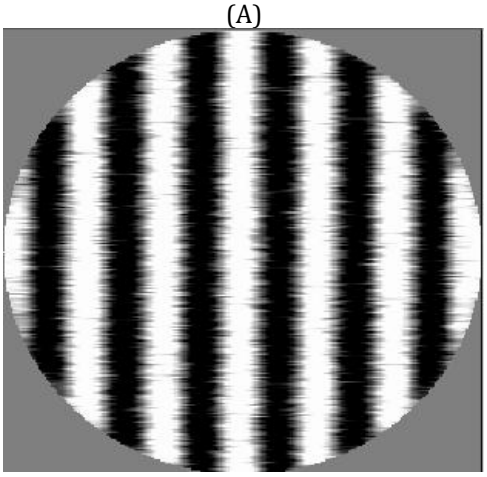

(B)

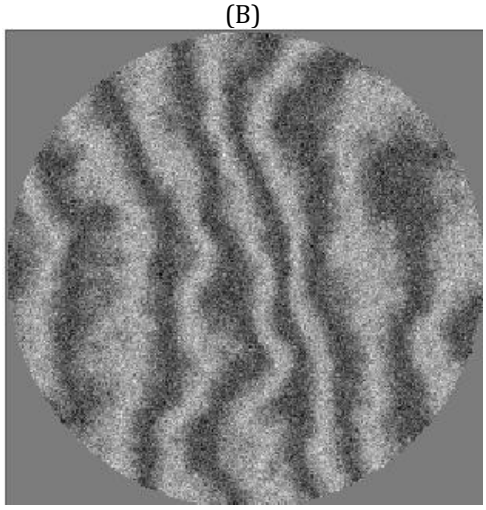

(C)

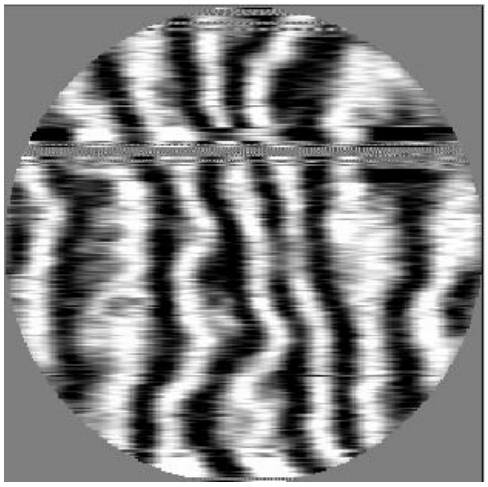

(D)

Figure 5: The noisy image and filtered image using windowed Fourier transform

V) Reconstruction of distorted wavefront

The phase thus recovered is measured with an integral multiple of 2π uncertainties. The process of removing these uncertainties is called phase unwrapping. After phase has been completely unwrapped, the data contains the derivatives of the original phase of the wavefront. The derivative of the wavefront phase can conveniently be written in terms of Zernike polynomials, to estimate the wavefront errors. The Zernike coefficients provide the complete information of the wavefront.

5.1 Wavefront determination from wavefront slope data using Zernike polynomial

The aberrated wavefront has to be reconstructed from the wavefront slopes derived from the above method. The wavefront aberrations can be well represented by Zernike polynomials. The derivatives of the Zernike polynomials can be expressed as a linear combination of Zernike polynomial [8]. They are written as

$$\Delta Z_j = \sum_{j'} \gamma_{jj'} Z_{j'} \tag{5.1}$$

Alternatively

$$\Delta\varphi = \sum_j \left(\sum_j a_j \gamma_{jj'} \right) Z_j \tag{5.2}$$

where $\gamma_{jj'}$ are the coefficients of the Zernike expansion of the derivative of the j[th] Zernike. The matrix γ is called Zernike derivative matrix and it is given in [13]. The wavefront slope as derived from this method can be written as in equation 5.3.

$$\Delta W(x,y) = \frac{\partial W}{\partial x} s + \frac{\partial W}{\partial y} t \tag{5.3}$$

where $\frac{\partial W}{\partial x}$ & $\frac{\partial W}{\partial y}$ correspond to the x and y derivatives of the wavefront slope. Therefore

$$\frac{\partial W}{\partial x} = \sum_j \left(\sum_j a_j \gamma^x_{jj'} \right) Z_j \quad \text{and} \quad \frac{\partial W}{\partial y} = \sum_j \left(\sum_j a_j \gamma^y_{jj'} \right) Z_j \tag{5.4}$$

So that combining (5.2), (5.3) and (5.4),

$$\Delta W(x,y) = s \sum_j \left(\sum_j a_j \gamma^x_{jj'} \right) Z_j + t \sum_j \left(\sum_j a_j \gamma^y_{jj'} \right) Z_j \tag{5.5}$$

In matrix notation this equation can be written as

$$W = A\,Z$$

W contains the values of the wavefront slope, **A** the Zernike coefficients which are to be determined and **Z** is the Zernike polynomial corresponding to the coefficients with a multiplicative factor of shear. The number of measurements is typically more than the number of unknowns, so a least square solution is useful. This over determined system is solved as follows:

$$\begin{aligned} W\ ZT &= A\,Z\,Z^T \\ W\ ZT\ (Z\,ZT)\text{-}1 &= A\,(Z\,Z^T)\,(Z\,Z^T)^{-1} \end{aligned}$$

$$A = W\ ZT\ (Z\,Z^T)^{-1} \tag{5.6}$$

A provides the Zernike coefficients. Using the Zernike coefficients, the aberrated wavefront is reconstructed as

$$W(x,y) = \sum_{j=2}^{N} a_j Z_j \tag{5.7}$$

Where a_j are the Zernike expansion coefficients. So far the considerations have involved, derivations based on the theory for ΔW_x and ΔW_y, with the resulting

polynomial expressions formulated in terms of circle of unit radius.

We explained the use of Zernike base phase screen for known and repeatable characteristics of turbulence generation in section 3. It also used to characterize the phase estimation, data reduction methods and error finding by comparing the input values of Zernike coefficients (which we used for generating Zernike based phase screen) and output values of Zernike coefficients (which we get after phase estimation and data reduction). The comparison of input Zernike values (phase screen with Zernike) and output Zernike values (here in wavefront reconstruction **A** provides the Zernike coefficients) depends on the performance of the phase extraction algorithm and data reduction method. In figure 6 a graph shows the comparison of input Zernike values with evaluated Zernike values of proposed WFT algorithms.

0.00
0.00
0.00
3.97
-3.7031
-2.7025
1.9528
1.3291
-2.7043
-2.7056
-0.6907

Table 3. Output Zernike Coefficients

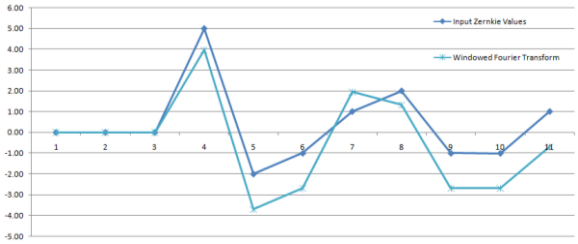

Figure 6: Zernike Comparison Graph

VI) CONCLUSION

In this paper we have developed a Zernike based interferogram and phase screen. We incorporated the phase screen into the interference fringe pattern and due to that the interference gets distorted. From the distorted fringe pattern, we extracted the phase using Window Fourier Transform. The extracted phase is unwrapped and fitted into Zernike polynomial to slope identification. The resultant Zernike values are compared with its input values.

VII) REFERENCE

[1]Hardy, J. W. (1998) "Adaptive Optics for Astronomical Telescopes. Oxford: Oxford University Press.

[2]Julie A. Perreault, Thomas G. Bifano, B. Martin Levine and Mark N. Horenstein "Adaptive optic correction using micro electro mechanical deformable mirrors", Optical Engineering, 41(3) 561-566, March 2002.

[3] Hardy, J.W. and Alan J. MacGovern., "Shearing interferometry: a flexible technique for wavefront measurement" SPIE, Vol. 816, "Interferometric Metrology",180–195(1987).

[4] J.W.Hardy, J.E.Lefebvre and C.L.Koliopoulous, "Real-time atmospheric compensation." J.Opt.Soc.Am. 67, 360-369 (1977).

[5] J.W.Hardy, "Adaptive Optics: a new technology for the control of light," Proc.IEEE 66, 651-697 (1978).

[6] A.K.Saxena and J.P.Lancelot, "Theoretical fringe profiles with crossed Babinet compensators in testing concave aspheric surfaces," Appl.Opt. 21, 4030-4032 (1982)

[7] A.K.Saxena and J.P.Lancelot, "Wavefront sensing and evaluation using two crossed Babinet compensators," SPIE, 1121, 41-43 (1990).

[8] Noll, R.J., "Zernike polynomials and atmospheric turbulence" J. Opt. Soc. Am., Vol. 66, No.3, 207 – 211 (1976).

[9] Harbers G, P.J.Kunst and G.W.R Leibbrandt, "Analysis of lateral shearing interferograms by use of Zernike polynomials", Appl.Opt. 35, No.31, 6162 – 6172 (1996).

[10] D. L. Fried. Statistics of a geometric representation of wavefront distortion. J. Opt. Soc. Am., 55(11):1427–1431, 1965.

[11] Qian Kemao "Windowed Fourier transform for fringe pattern analysis", APPLIED OPTICS _ Vol. 43, No. 13 _ 1 May 2004

[12] Qian Kemao, Haixia Wang, and Wenjing Gao "Windowed Fourier transform for fringe patternanalysis: theoretical analyses", APPLIED OPTICS / Vol. 47, No. 29 / 10 October 2008.

[13] Kemao Qian,_, Seah Hock Soon, Anand Asundi, "A simple phase unwrapping approach based on filtering by windowed Fourier transform", Optics & Laser Technology 37 (2005) 458–462, Elsevier Ltd.

[14] S. Mallat, A Wavelet Tour of Signal Processing, 2nd ed. _Academic, San Diego, 1999_.

[15] K. Krochenig, Foundations of Time–Frequency Analysis _Birkha¨user, Boston, 2001_.